International Journal of Engineering and Technology Innovation, vol. 8, no. 4, 2018, pp. 307 - 320

A Reliable QRS Detection Method Based on Dual-Tree Wavelet Transform

Oussama El B'charri[1,*], Rachid Latif[1], Abdenbi Abenaou[1], Khalifa Elmansouri[2], Wissam Jenkal[1]

[1]ESSI-LISTI Laboratory, National School of Applied Sciences, Ibn Zohr University, Agadir, Morocco

[2]High School of Biomedical Engineering; UM6SS University, Casablanca, Morocco

Received 31 July 2017; received in revised form 27 March 2018; accepted 05 April 2018

Abstract

Electrocardiography is considered as a powerful technique for assessing heart condition. To study cardiac disorders, it is essential to localize and extract the QRS complex: the prominent region within the electrocardiogram signal. Since the QRS complex has various morphologies and is usually contaminated by severe overlapping spectral noise, accurate detection is a complicated task. This paper proposes a reliable method based on the Dual-Tree Wavelet Transform, which uses a threshold process to select the QRS frequency components and reduce the overlapping noise. The QRS deflections are then emphasized using squaring and moving average operators. The chosen decision rule is simple and based on the variance of the signal. The proposed method was tested on the MIT-BIH Arrhythmia database, and the algorithm showed high accuracy detection results compared to those of other recently published works.

Keywords: ECG signal, QRS complex, dual tree wavelet transform

1. Introduction

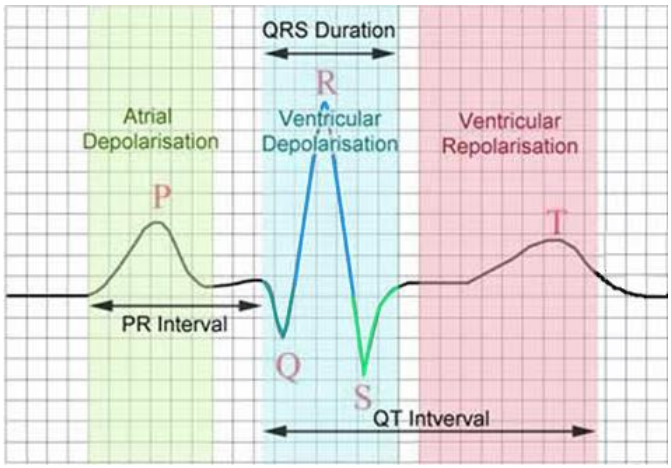

Fig. 1 A normal ECG waveform [1]

The electrocardiogram (ECG) is a transthoracic representation of the heartbeat's electrical activity over time. It is a non-invasive technique used by physicians to monitor and control heart activity in a clinical setting. The ECG trace covers various components that are represented by P-QRS-T waves [1], as shown in Fig. 1. Starting from the first deflection (the P-wave), it is produced from atrial depolarization and lasts up to 0.12 s. Next comes the QRS complex: the most important feature and largest component of the ECG signal. The QRS complex begins with the Q-onset and ends with the S-offset. It

* Corresponding author. E-mail address: el.bcharri@gmail.com
Tel.: +212-676-679367

results from the electrical forces engendered by ventricular depolarization. The normal duration of the QRS complex is up to 0.1 s. When ventricular repolarization occurs, the T wave appears and remains for about 0.18 s [2].

All clinical features are essential to physicians seeking to recognize and diagnose heart conditions, in particular, the temporal localization of the QRS complex. The identification of QRS subfractions mediated by its mathematical signal decomposition is of particular utility for semiautomatic devices delivering therapies that require proper identification. Thanks to recent emerging technologies that offer efficient computational tools, numerous complex diagnostic and prognostic tasks can be implemented to help physicians in their practice and interpretation. However, the proper detection of QRS subfractions is not a simple undertaking, as the ECG signal is usually corrupted by various background noises. Moreover, the heartbeat could change the shape and characteristic patterns that are due to the various morphologies of normal and abnormal ECG traces. A high-precision QRS complex recognition algorithm that is able to identify various QRS subfractions, even in the presence of noise, is hence required. A large number of studies have focused on detecting and extracting the QRS complex. Tompkins [3-4] carried out some early work in this field. Recent research has been based on mathematical models [5], sparse derivatives [6], entropy [7], filtering techniques [8], correlation analysis [9], and kurtosis [10]. Many of the latest methods are based on the discrete wavelet transform (DWT) [11–15], as it can detect local, transient or intermittent components in the ECG signal. To further minimize computation time, researchers [16,17] have investigated the DWT in both ECG noise removal and ECG features delineation, based on an optimal selection of wavelet functions and decomposition levels. While favorable outcomes have been achieved, the DWT has several drawbacks in important areas such as oscillations around singularities, shift variance, aliasing, and lack of directionality [18,19]. The dual-tree wavelet transform (DT-WT) has been utilized to overcome these limitations and to provide an efficient QRS detection algorithm.

In the present work, a reliable QRS detection method is proposed based on the DT-WT. The signal was decomposed into multi-resolution levels to select the most prominent frequency band of the QRS complex. A threshold criterion was applied to reduce the overlapping noise within the QRS regions. These regions were then boosted using simple operations. The decision rule was computed from the variance of the obtained signal. The paper is structured as follows: Section 2 gives the theoretical background of the wavelet domain and explains the reasons for using the DT-WT. Section 3 describes the proposed algorithm. The results are presented and discussed in Section 4. And Section 5 is the conclusion.

2. The Comprehensive Theoretical Basis

2.1. Conventional wavelet transform

Since its inception, the Wavelet Transform (WT) has become the most powerful tool for analyzing signals and images in many fields of research. Unlike the traditional Fourier Transform (FT), the WT is a time-frequency analysis method that can detect local, transient or intermittent components in the studied signal. The transformation is linear, allowing a signal to be refined into multi-resolution representations using a scaled and shifted form of the mother wavelet. The continuous form of this transform was initially formulated in the 1980s by Grossman and Morlet [20]. The Continuous Wavelet Transform (CWT) is expressed by a set of the inner product of the studied signal $x(t)$, with the shifted and scaled prototype wavelet [21]:

$$CWT_x^{\psi}(a,\tau) = \Psi_x^{\psi}(a,\tau) = \frac{1}{\sqrt{|a|}} \int x(t)\psi^*(\frac{t-\tau}{a})dt \tag{1}$$

The transformed signal is a function of two variables, a and τ, that represent the scale and translation parameters of the mother wavelet $\psi(t)$, respectively. Nowadays, the discrete version of this transform is widely used in digital systems,

including embedded systems. The DWT is sampled from the CWT by setting $a = a_0^j$ and $\tau = ka_0^j\tau_0$ where j and k are integers and $a_0 > 1$ is a real number. For practical implementation reasons, these variables are adjusted on a dyadic grid such as $a = 2^j$ and $\tau = k2^i$. The mother wavelet becomes [21]:

$$\psi_{j,k}(t) = 2^{(-\frac{j}{2})}\psi(2^{-j}t - k) \tag{2}$$

The expression of the Eq. (2) finds its similarity in the filter bank (FB) theory [22]:

$$a_n^{(j)} = \sum_{k=0}^{N-1} g(2n-k)a_{j-1}(n) \tag{3}$$

$$d_n^{(j)} = \sum_{k=0}^{N-1} h(2n-k)a_{j-1}(n) \tag{4}$$

Here, Eqs. (3) and (4), which represent the approximation and detail coefficients of the WT, are associated with the high pass $g(n)$ and low pass $h(n)$ filters, respectively. The signal is down-sampled by two at each level j of the decomposition. The approximation sequence of a level j is used as an input to the next decomposition level ($j+1$).

2.2. *Drawbacks of the discrete wavelet transform*

Despite its success in several areas of research, the DWT suffers from the following four shortcomings: oscillations, shift variance, aliasing and lack of directionality. These issues are illustrated and explained in detail in [23]. We give a brief description of each of these inconveniences. The oscillations problem occurs when the signal contains singularities. In Fig. 2, we took a unit impulse signal as the input signal. Computing the real DWT detail coefficients of the third decomposition level, we observed that the output wavelet coefficients tend to oscillate between positive and negative around this singularity.

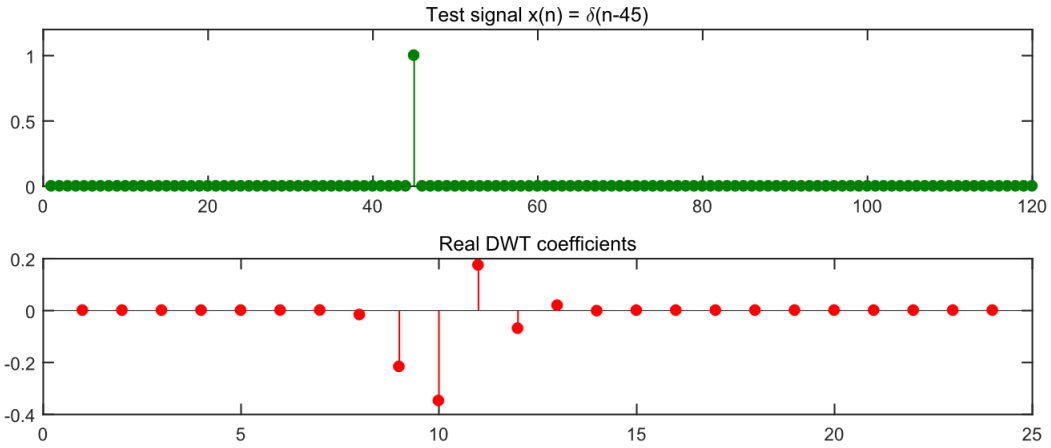

Fig. 2 The DWT coefficient oscillations due to singularity

Shift variance is another serious problem that can lead to significant changes in the output DWT coefficients when time shifting the input signal. To illustrate this shortcoming, a shift variability test was applied to an input step signal [24]. A multiresolution analysis was then performed to the input step signal, as shown in Fig. 3. Clearly, the DWT coefficients (on the right) were sensitive to small translations of the signal. However, the DT-WT coefficients (on the left) were nearly shift-invariant. The aliasing problem of the DWT is caused by the use of non-ideal high pass and low pass filters, which compute the wavelet coefficients by a series of discrete-time down-sampling operations, producing other unwanted frequency components at each decomposition level. This problem is especially apparent when processing wavelet coefficients, as in the case of the threshold step. Lastly, the DWT lacks directionality. This issue concerns the multidimensional DWT, as in the case of image processing. Given that our work here involves a one-dimensional signal, however, we will not be discussing this shortcoming.

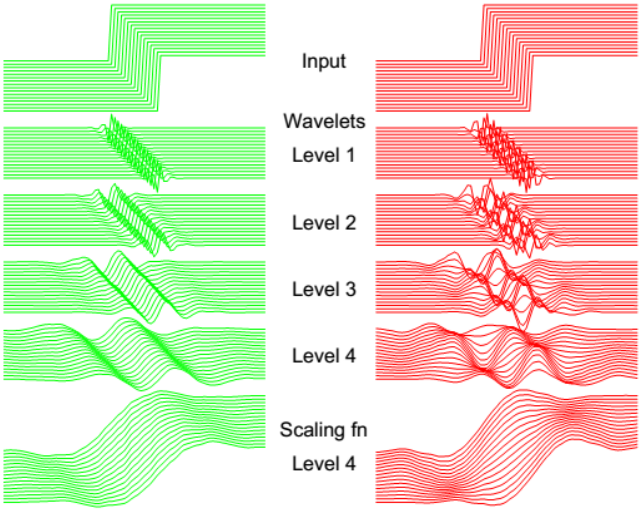

Fig. 3 DT-WT and DWT against shift variability test [24]

2.3. *The dual tree wavelet transform*

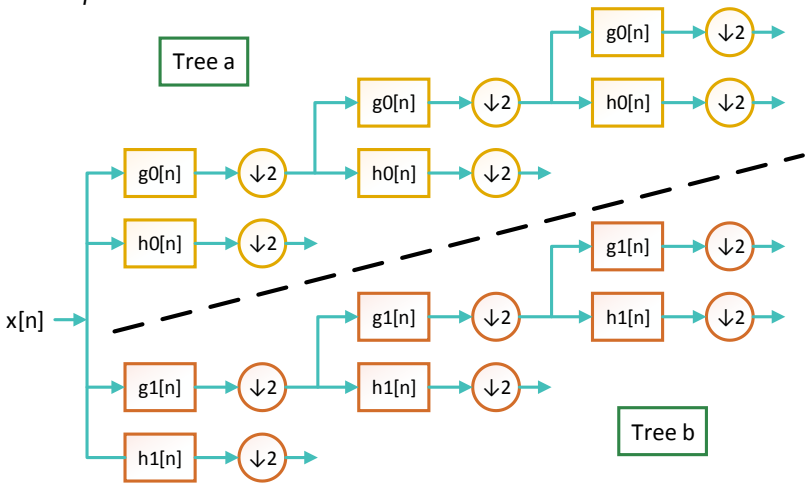

Fig. 4 Flowchart of the analysis FB used in DT-WT

Kingsbury [24] was the first to introduce the Dual-Tree Wavelet Transform (DT-WT). One of the most improved versions of the DWT, the DT-WT offers new fundamental properties that overcome the limitations encountered by the DWT. Unlike the conventional DWT, the DT-WT is constructed using two separate real filters to give an analytic transform, as shown in Fig. 4. The real part of the complex wavelet coefficients is given by the first tree, while the second tree is responsible for the imaginary part. The idea behind the complex transform of this wavelet is based on the FT representation expressed as:

$$\psi(t) = \psi_h(t) + i\psi_g(t) \tag{5}$$

with magnitude

$$|\psi(t)| = \sqrt{|\psi_h(t)|^2 + |\psi_g(t)|^2} \tag{6}$$

and phase

$$\angle\psi(t) = \arctan\left(\frac{\psi_g(t)}{\psi_h(t)}\right) \tag{7}$$

where $i = \sqrt{-1}$, $\psi_h(t)$ is real and even whereas $\psi_g(t)$ is imaginary and odd. These are implemented so that $\psi_g(t)$ is the Hilbert transform of $\psi_h(t)$, ensuring the perfect reconstruction of the decomposed signal.

3. Research Method

We propose a reliable method based on the DT-WT by which to accurately detect the QRS regions. Fig. 5 shows the process involved. Each step of the flowchart is explained in detail by the following subsections:

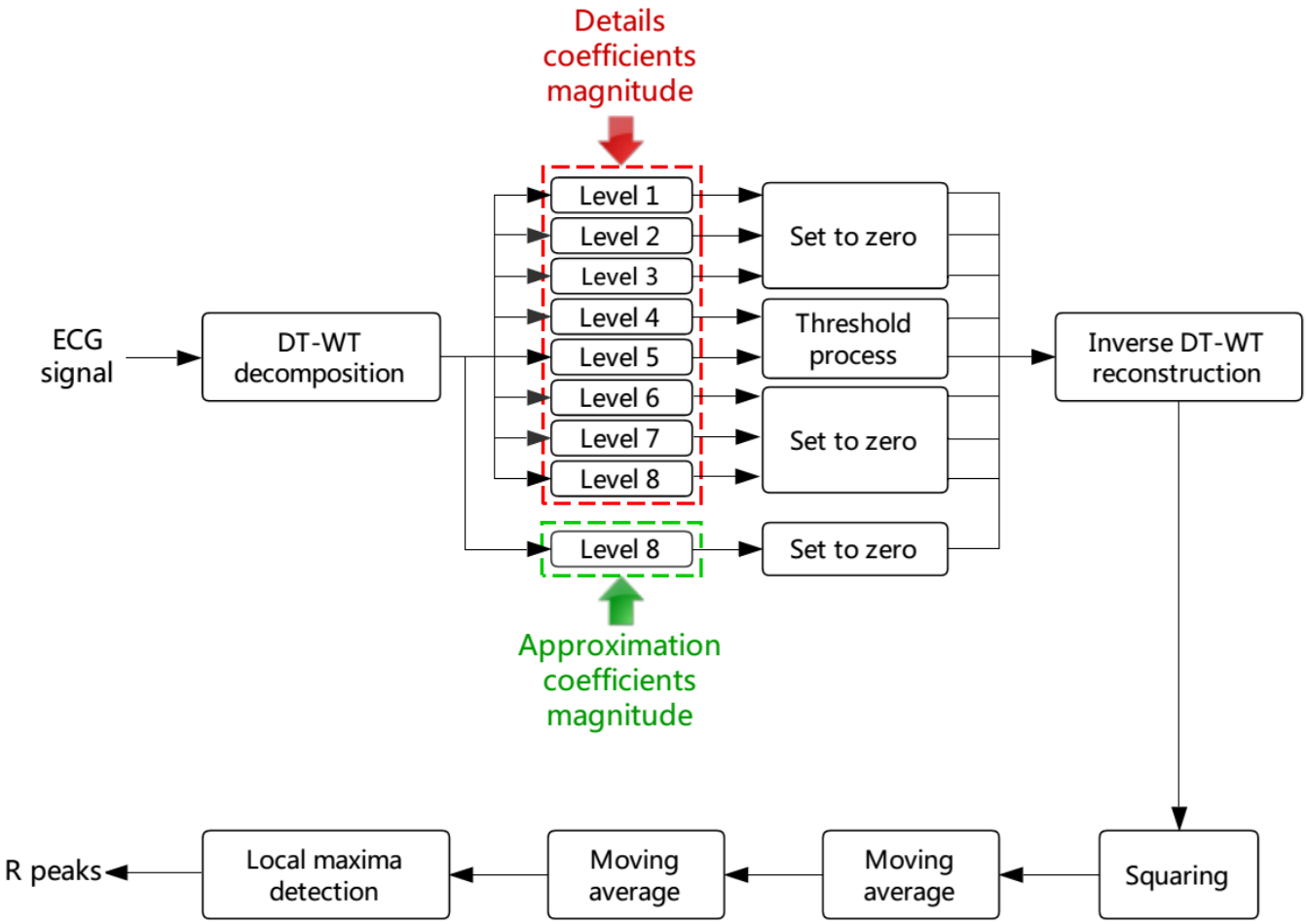

Fig. 5 Flowchart of the proposed method

3.1. *ECG signal decomposition*

The ECG signal was decomposed up to a specific level, depending upon the Baseline Wandering (BW) frequency and the sampling frequency. The selected decomposition level L was calculated from the equation (8) [25], where $f_{BW}(=1Hz)$ represents the maximum frequency value that can reach the BW noise, and $F_{\max}$ is the highest frequency components in the ECG signal that respects the Nyquist's theorem. Here, $ceil$ is the ceiling function that gives the smallest integer greater than or equal to the result.

$$L = ceil(\log_2(\frac{F_{\max}}{f_{BW}})) \tag{8}$$

3.2. *Threshold of the DT-WT coefficients magnitude*

According to [14], most of the QRS complex frequency components of both normal and abnormal beats are concentrated between 5-22 Hz, which corresponds to the DT-WT decomposition levels 4 and 5 for a sampling rate of 360 Hz. Unfortunately, ECG signals are contaminated by several noises that overlap the QRS frequency band. Hence, the threshold process of these two levels is of paramount importance. A comprehensive study [18] recently stated that the impact of the choice of threshold estimators, threshold value, and the appropriate wavelet decomposition level to remove different types of artifacts. In this work,

we tested all the threshold estimators, with the Hard function found to be the best option. The magnitude of the detail coefficients of levels 4 and 5 was quantified according to the following formula, given in [26]:

$$Th_j = \sigma_j \frac{\sqrt{2\log(N)}}{\log(j+1)} \tag{9}$$

where N denotes the length of the original ECG signal, σ_j is the standard deviation of the *j*-th decomposition level (4 and 5) expressed as [27]:

$$\sigma_j = \frac{MAD(|M_{d,j}|)}{0.6745} \tag{10}$$

Here, MAD represents the median absolute deviation of the detail coefficients magnitude $M_{d,j}$.

The remaining decomposition levels were set to zero, as they fell outside of the QRS frequency band. It should be noted here that the eighth approximation level was also set zero to eliminate baseline shift from the signal.

3.3. The reconstructed waveform

All the processed detail coefficients, along with the approximation coefficients, were then used to reconstruct the signal. The reconstructed waveform was obtained by using the inverse DT-WT on the decomposed threshold coefficients. To clarify this step, Fig. 6 shows an ECG signal with baseline drift collected from a segment of record n°113 (160-180 s) from the MIT-BIH Arrhythmia database. We performed the steps described in subsections 3.1 and 3.2 to provide the threshold eight-detail coefficients magnitude and the corresponding approximation coefficients magnitude. The reconstructed waveform given in Fig. 6 was acquired by applying the inverse DT-WT to the modified coefficients.

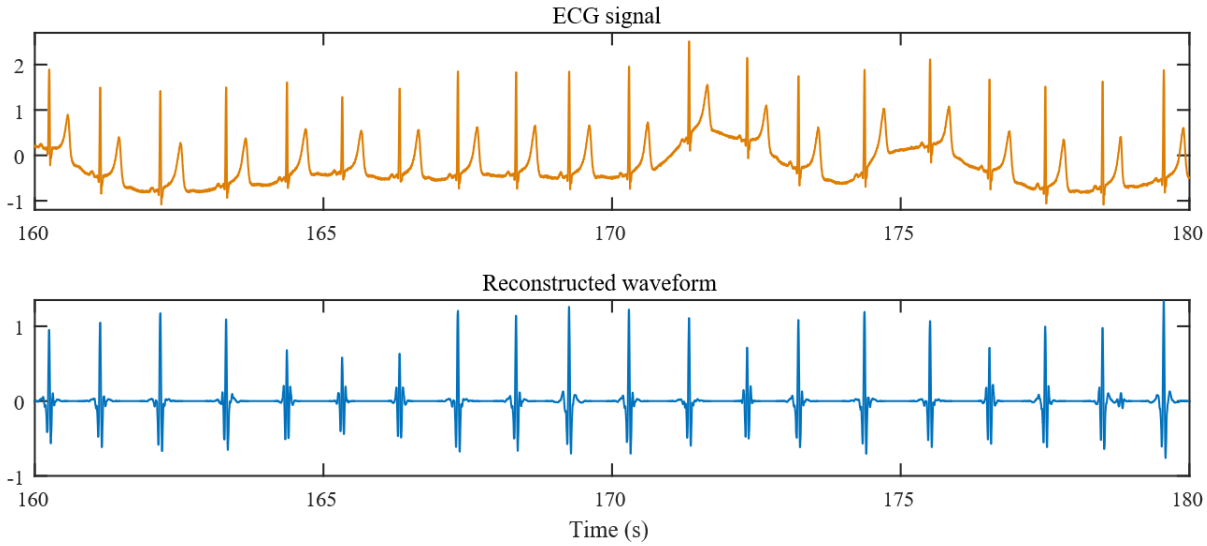

Fig. 6 The reconstructed waveform from the inverse DT-WT reconstruction step

3.4. Squaring and moving average operators

To localize the QRS region, the reconstructed waveform required further processing. The squaring stage (a nonlinear operation) was used to emphasize the beats and reduce the remaining noises. All the samples in this step had positive values. The signal was then smoothed by using two cascade moving average windows. The width of these two windows was selected in accordance with the physiological refractory inter-beat interval of 200 ms, which is approximately equal to 75 samples in the case of a sampling frequency of 360 Hz. As shown in Fig. 7, using only one moving average window is insufficient, as the

output signal at this stage has flat extrema. Thus, the second moving average window was necessary to boost the localization of peaks. The obtained signal at this stage was shaped like the envelope of the reconstructed waveform.

3.5. *Local maxima detection*

Finally, the algorithm's last step was to extract the QRS regions. Normally, a threshold value is used to identify the accurate beats. This value is selected carefully according to the developed algorithm. For this technique, the variance of the obtained signal was used as a threshold criterion, expressed as:

$$T = \frac{1}{N-1}\sum_{i=1}^{N}\left|x_i - \bar{x}\right|^2 \tag{11}$$

where x_i denotes the samples of the obtained signal length of N and $\bar{x}$ represents the mean of this signal.

Once the threshold value was confirmed, the minimum peak distance was chosen empirically as 150 samples covering nearly the entire triangle-like shape in the envelope. Finally, the threshold value and the minimum peak distance are used as two input parameters to determine the R peaks.

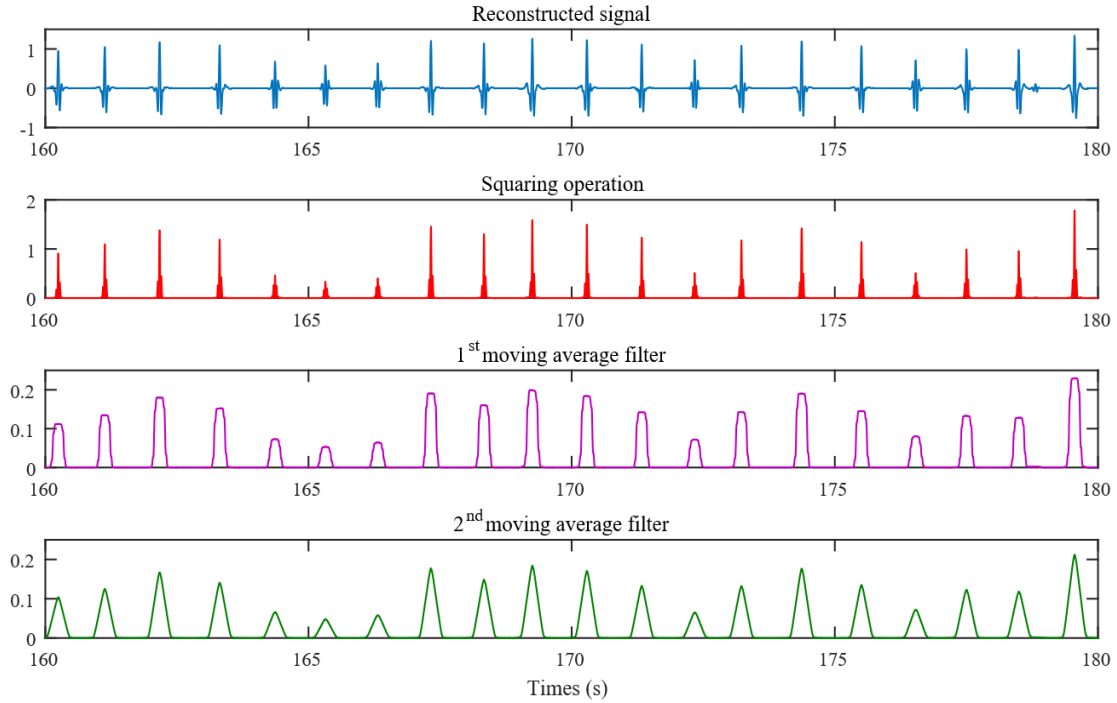

Fig. 7 Waveforms obtained from squaring and moving average operators

4. Results and Discussion

To analyze the performance of the proposed algorithm and to compare the results with other works, it was necessary to investigate a standard database. The outcome of the algorithm should also be verified by an annotated database that has been previously assessed by expert cardiologists. For these reasons, the MIT-BIH Arrhythmia Database [28] comprised of 48 records sampled at a frequency of 360 Hz with 11-bit resolution over a range of 10 mV was selected. The whole dataset was tested for the proposed method, except for recording n° 207, from which a duration of 142.5 s was excluded due to Ventricular Flutter (VF) intervals [14]. Comparison between the estimated R peaks location and the annotation file were performed by using the ECG-kit toolbox developed by Demski [29].

4.1. Statistical evaluation metrics

To validate the detection effectiveness and to demonstrate the quality of the analysis, it was necessary to refer to the statistical parameters able to describe the reliability of the proposed method. These metrics – sensitivity, positive predictivity, and detection error – were defined, respectively, as:

$$Se(\%) = \frac{TP}{TP + FN} \times 100 \tag{12}$$

$$PP(\%) = \frac{TP}{TP + FP} \times 100 \tag{13}$$

$$DER(\%) = \frac{FP + FN}{TB} \times 100 \tag{14}$$

where *TP* is the correctly recognized detected beats (True Positive) and *FN* the correctly undetected beats (False Negative). *FP* is falsely detected beats (False Positive), and *TB* represents the total annotated beats in the analyzed ECG signal.

4.2. Evaluation of results and discussion

Using all of the previously described parameters, the proposed method was evaluated using the entire MIT-BIH Arrhythmia database records. The algorithm was implemented using MATLAB R2016b software. Table 1 summarizes the algorithm performance under the given statistical metrics. The total beats considered in each record is also given. For each record, the total beats were taken in respect to the maximum number of samples that could be used according to the wavelet dyadic length decomposition. Table 1 shows that almost all records had excellent results, with the exception of records such as 116, 203, 208 and 232. The reasons for the bad R peaks localization in these records will be discussed in the suitable course.

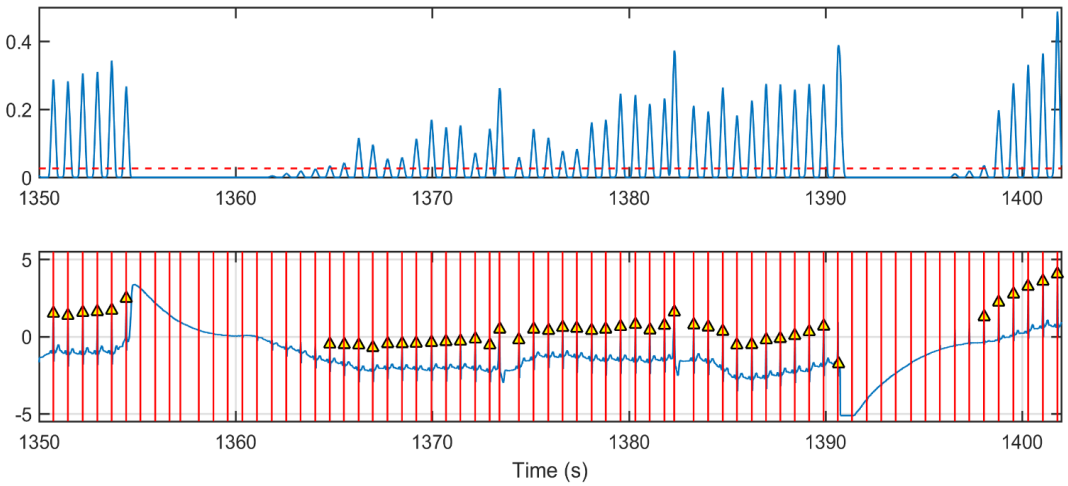

Fig. 8 Delineation of R peaks for ECG record 116 from the MIT-BIH Arrhythmia database

Before we demonstrate the results qualitatively by illustrating some ECG signals (Figs. 8-16), we should clarify the representation used in the Figures. The top subplot denotes the resulting waveform and the corresponding threshold indicated by dotted line (--). The bottom subplot represents R peaks localization (Δ) found by our algorithm versus the cardiologists' annotation delineated by vertical lines (|). As shown in Fig. 8, the number of false negative beats presented in record 116 were mainly caused by small, almost invisible beats that were under the threshold level. Record 203 was corrupted by high-frequency noise, and had a significant number of multiform premature ventricular complexes, producing the remarkable FN. However, the detection error in this record was greatly reduced comparing with other recently published methods [5,7,8,10]. Record 208 also contained some small amplitude beat pulses and a very short inter-beat interval, leading to detection errors. The high number of false positive beats observed in record 232 was due to QRS-like artifacts.

Table 1 QRS detection results for the MIT-BIH Arrhythmia database

Tape	Total beats	TP	FP	FN	Se(%)	PP(%)	DER(%)
100	2,272	2,272	0	0	100.00	100.00	0.00
101	1,865	1,865	0	0	100.00	100.00	0.00
102	2,187	2,187	0	0	100.00	100.00	0.00
103	2,084	2,084	0	0	100.00	100.00	0.00
104	2,229	2,228	3	1	99.96	99.87	0.18
105	2,572	2,570	3	2	99.92	99.88	0.19
106	2,027	2,019	1	8	99.61	99.95	0.44
107	2,137	2,135	0	2	99.91	100.00	0.09
108	1,763	1,761	4	2	99.89	99.77	0.34
109	2,532	2,532	0	0	100.00	100.00	0.00
111	2,124	2,123	0	1	99.95	100.00	0.05
112	2,539	2,539	0	0	100.00	100.00	0.00
113	1,794	1,794	0	0	100.00	100.00	0.00
114	1,879	1,879	3	0	100.00	99.84	0.16
115	1,953	1,952	0	1	99.95	100.00	0.05
116	2,412	2,387	0	25	98.96	100.00	1.04
117	1,535	1,535	2	0	100.00	99.87	0.13
118	2,278	2,278	0	0	100.00	100.00	0.00
119	1,987	1,987	0	0	100.00	100.00	0.00
121	1,863	1,863	1	0	100.00	99.95	0.05
122	2,476	2,476	0	0	100.00	100.00	0.00
123	1,518	1,518	0	0	100.00	100.00	0.00
124	1,619	1,619	0	0	100.00	100.00	0.00
200	2,601	2,600	2	1	99.96	99.92	0.12
201	1,963	1,962	0	1	99.95	100.00	0.05
202	2,136	2,135	0	1	99.95	100.00	0.05
203	2,980	2,957	1	23	99.23	99.97	0.81
205	2,656	2,655	0	1	99.96	100.00	0.04
207	1,860	1,858	2	2	99.89	99.89	0.22
208	2,955	2,933	1	22	99.26	99.97	0.78
209	3,005	3,005	0	0	100.00	100.00	0.00
210	2,650	2,648	1	2	99.92	99.96	0.11
212	2,748	2,747	0	1	99.96	100.00	0.04
213	3,250	3,244	0	6	99.82	100.00	0.18
214	2,262	2,256	0	6	99.73	100.00	0.27
215	3,363	3,363	0	0	100.00	100.00	0.00
217	2,208	2,204	0	4	99.82	100.00	0.18
219	2,154	2,154	0	0	100.00	100.00	0.00
220	2,048	2,047	0	1	99.95	100.00	0.05
221	2,427	2,427	0	0	100.00	100.00	0.00
222	2,483	2,483	2	0	100.00	99.92	0.08
223	2,605	2,604	0	1	99.96	100.00	0.04
228	2,053	2,048	9	5	99.76	99.56	0.68
230	2,256	2,256	0	0	100.00	100.00	0.00
231	1,571	1,571	0	0	100.00	100.00	0.00
232	1,780	1,780	19	0	100.00	98.94	1.07
233	3,079	3,071	0	8	99.74	100.00	0.26
234	2,753	2,753	0	0	100.00	100.00	0.00
Total	109,491	109,364	54	127	99.90	99.94	0.16

It should be noted that the proposed algorithm did bring good results for record 105, which usually has a significant error rate in the majority of detection methods found in the literature. This performance can be seen in Fig. 9, which illustrates the detection accuracy of the algorithm for record 105, even in the presence of high background noise. Fig. 10 shows a portion of record 104 that has severe muscle artifacts. Even with a high signal-to-noise ratio, the proposed algorithm was able to easily eliminate these artifacts. Fig. 11 illustrates another ECG scenario taken from record 201. This record presents not only

variations in the inter-beat intervals, but also a very small amplitude of some QRS complexes. Despite these variations, the proposed method was able to efficiently localize the QRS complexes. The additional window used in the resulting waveform of Fig. 11 zooms into a small QRS complex to demonstrate the important role of threshold value selection.

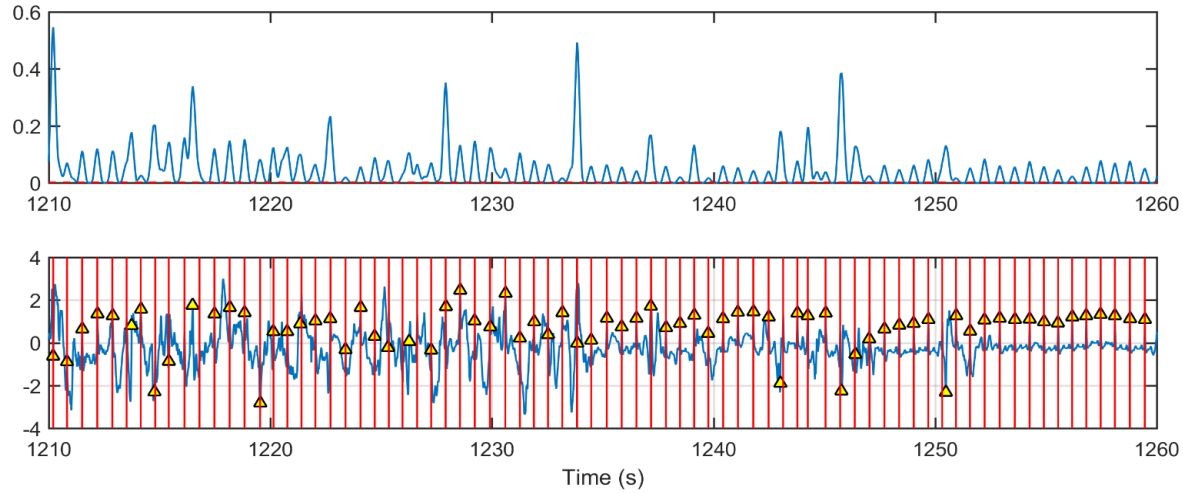

Fig. 9 Delineation of R peaks for ECG record 105 with artefacts from the MIT-BIH Arrhythmia database

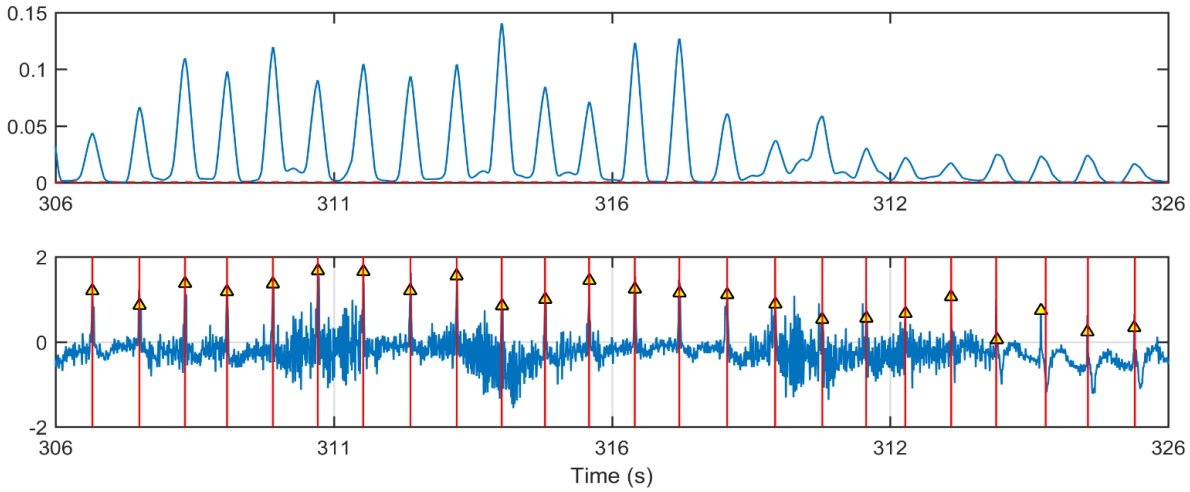

Fig. 10 Delineation of R peaks for ECG record 104 with muscle artifacts from the MIT-BIH Arrhythmia database

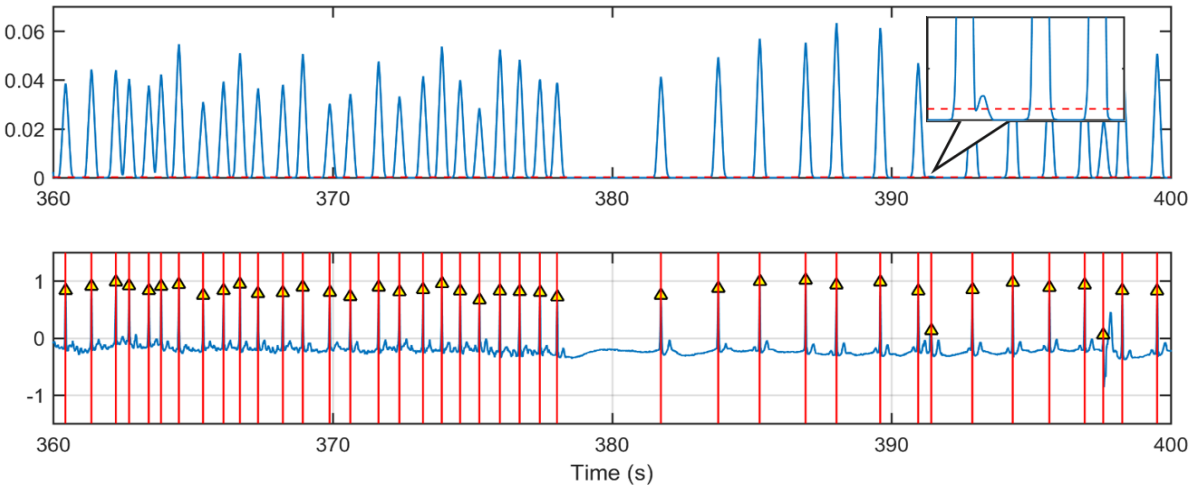

Fig. 11 Delineation of R peaks for ECG record 201 with small peaks from the MIT-BIH Arrhythmia database

The ECG records shown in Figs. 12-16 represent various arrhythmia ECG signals. The visual QRS subfractions detection is also given. Fig. 12 shows our method's QRS subfractions detection for a segment of the Atrial Fibrillation (AF) arrhythmia record 217 containing a fusion of paced beat and normal beat, as well as premature ventricular contraction. A run of

Ventricular Tachycardia (VT) taken from record 207, which has a mixture of Left Bundle Branch Block (LBBB) and Right Bundle Branch Block (RBBB), is illustrated in Fig. 13. The ECG signal for record 200 is another case of VT sequence along with ventricular bigeminy. The detection of QRS subfractions for this record is given in Fig. 14. Our algorithm is able to detect QRS subfractions even when the ECG signal presents a fusion of ventricular and normal heartbeat, as shown in Fig. 15. Another ECG scenario presenting ventricular tachycardia and atrial fibrillation taken from record 221 was tested on our algorithm, as shown in Fig. 16. Hence, our algorithm is able to handle a variety of ECG arrhythmias, moreover, we can affirm that our method has the capacity to be of clinical use in the future.

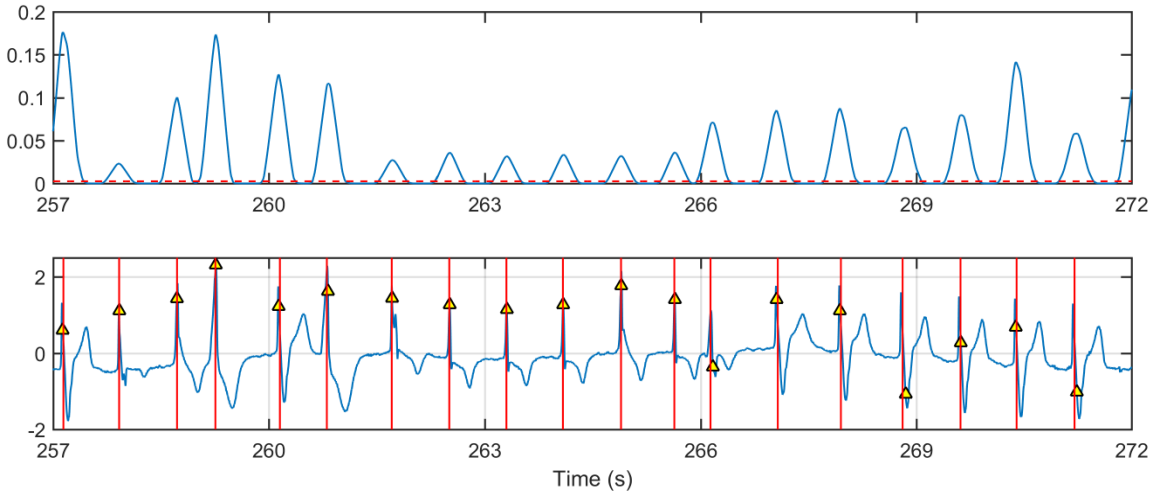

Fig. 12 Delineation of R peaks for ECG record 217 from the MIT-BIH Arrhythmia database

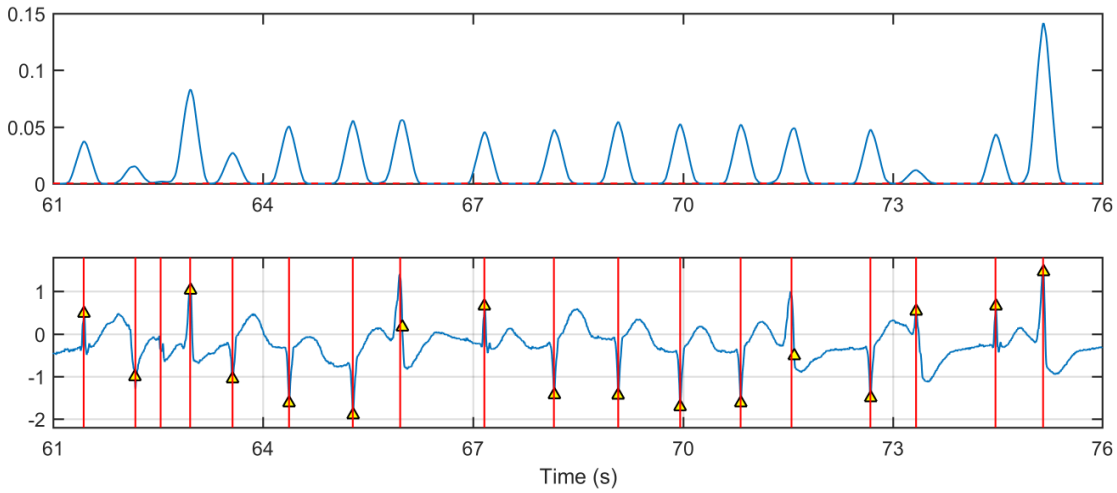

Fig. 13 Delineation of R peaks for ECG record 207 from the MIT-BIH Arrhythmia database

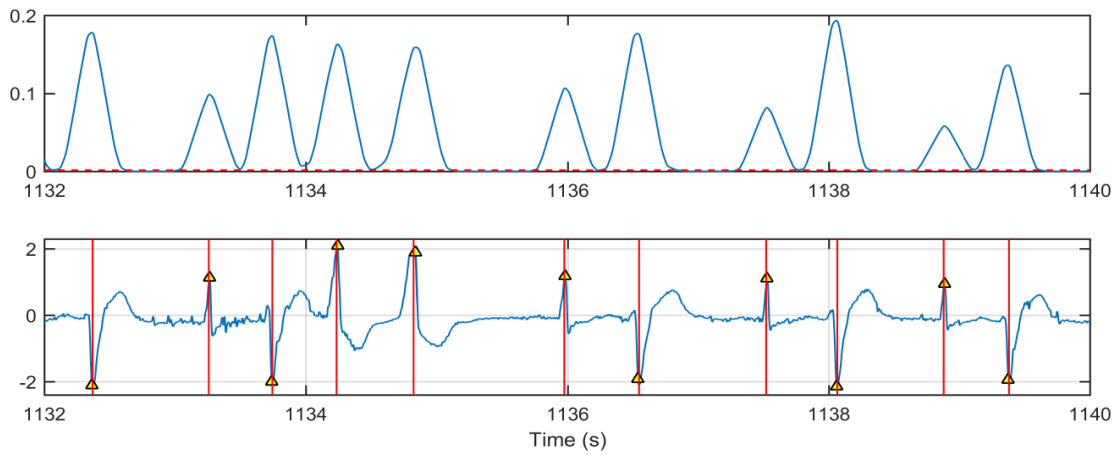

Fig. 14 Delineation of R peaks for ECG record 200 from the MIT-BIH Arrhythmia database

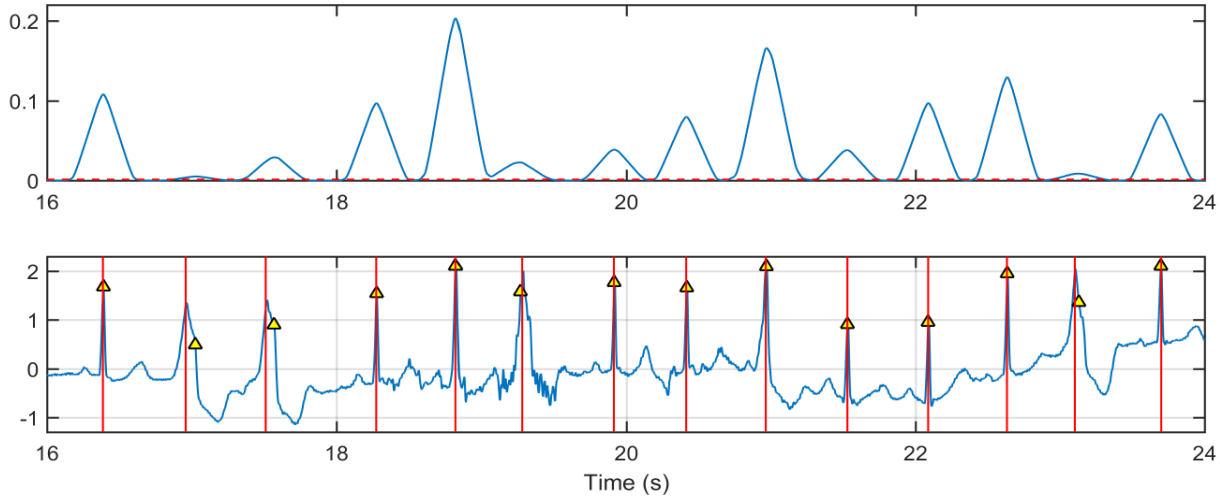

Fig. 15 Delineation of R peaks for ECG record 208 from the MIT-BIH Arrhythmia database

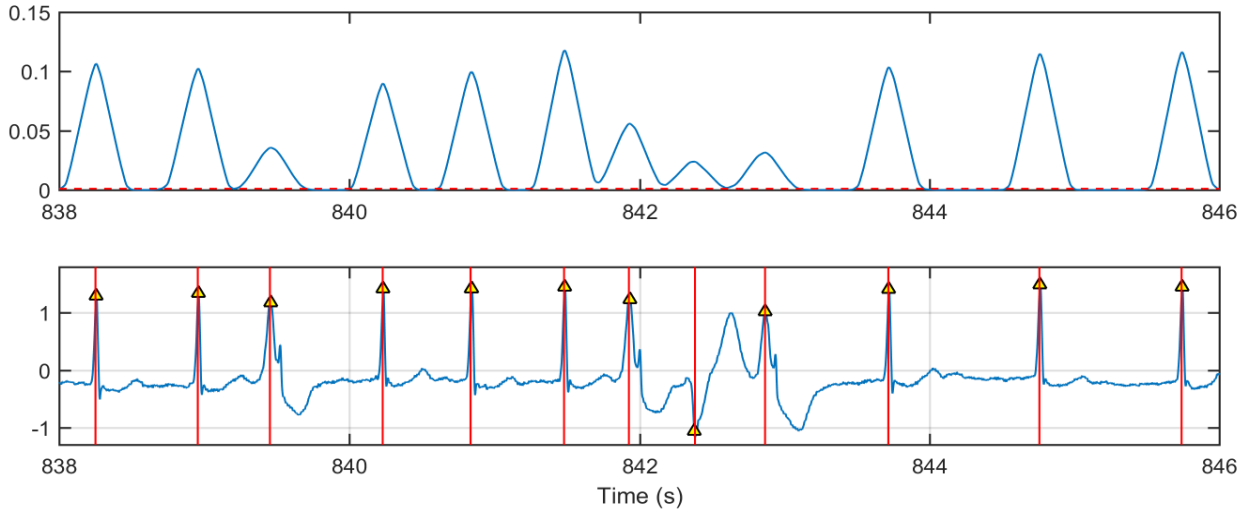

Fig. 16 Delineation of R peaks for ECG record 221 from the MIT-BIH Arrhythmia database

4.3. Performance comparison of the proposed QRS detection method

Table 2 Performance comparison with conventional and recently published high-quality QRS detection methods

Method	Year	Total beats	TP	FP	FN	Se(%)	PP(%)	DER(%)
[3]	1985	109,809	109,532	507	277	99.75	99.54	0.71
[4]	1986	109,267	108,927	248	340	99.69	99.77	0.54
[5]	2016	109,494	-	108	137	99.87	99.90	0.22
[6]	2013	109,452	109,314	127	138	99.87	99.88	0.24
[7]	2016	109,965	-	163	273	-	-	0.39
[8]	2015	109,494	-	353	614	99.43	99.67	0.88
[10]	2016	109,488	-	428	509	99.50	99.56	0.93
[12]	2014	116,137	-	308	192	99.81	99.70	0.49
[14]	2012	109,494	109,101	193	393	99.64	99.82	0.54
[15]	2012	19,098	19,022	76	40	99.60	99.50	-
[30]	2012	109,495	108,568	856	928	99.15	99.18	1.69
[31]	2016	109,491	109,331	574	160	99.85	99.48	0.67
[32]	1995	104,184	104,070	65	112	99.89	99.94	0.17
Proposed	2017	109,491	109,364	54	127	99.90	99.95	0.16

To provide a rigorous performance comparison, the results acquired from the proposed method should be set alongside various conventional QRS detection methods and recently published high-quality QRS detection methods. The database we used was the same as that of the comparative proposals. Although the work from [15] used a minimal number of resources from the MIT-BIH Arrhythmia database, we have included it as a reference for comparison purposes. The statistical metrics results in Table 2 demonstrate the robustness and reliability of the proposed algorithm. The recently introduced mathematical

detection model in [5], which surpasses that of other works, is comparable to our method. However, it is clear that the proposed method achieves a high performance since the number of undetected beats FN of our algorithm is smaller than the FN found in [5]. Furthermore, the number of falsely detected beats FP is very low comparing to all the other listed works, including the method used in [15] that was analyzed for minimal beats. The attained detection error value, which evaluates the overall accuracy of the algorithm, was lower than the methods cited in Table 2 (0.16%). Thus, we can assert that the proposed method succeeds in achieving high detection accuracy. Interestingly, the method is able to adapt to the non-stationarity nature of the ECG signal. Similarly, it is capable of detecting the QRS complex components with different morphologies, even in some challenging ECG data scenarios. What's more, it can hence be used in situations where ECG data from only one lead is available, such as in an ambulatory ECG.

5. Conclusions

A robust and reliable method based on DT-WT was proposed to detect the QRS complexes in ECG signals. First, the ECG signal was refined into a multi-resolution representation. Then, levels containing QRS frequency components were retained while the other levels were discarded. To emphasize the beats and reduce the remaining noise, the ECG signal was further processed using squaring and moving average operators. The decision rule used was simple and robust, making the extraction of various QRS morphologies possible. The whole MIT-BIH Arrhythmia database was investigated to test and compare the proposed algorithm with other works. The performance of the QRS detection method achieved high results comparing to existing methods, with a sensitivity of 99.88%, a positive predictivity of 99.95% and a detection error of 0.16%.

References

[1] myVMC, "ECG (electrocardiogram) heartbeat monitoring information," https://www.myvmc.com/investigations/ecg-ekg-electrocardiogram/, December 19, 2017.
[2] F. Morris, W. J. Brady, and A. J. Camm, ABC of clinical electrocardiography, 2nd ed. Chicester: John Wiley & Sons, June 2008.
[3] J. Pan and W. J. Tompkins, "A real-time QRS detection algorithm," IEEE Transactions on Biomedical Engineering, vol. 32, no. 3, pp. 230-236, March 1985.
[4] P. S. Hamilton and W. J. Tompkins, "Quantitative investigation of QRS detection rules using the MIT/BIH arrhythmia database," IEEE Transactions on Biomedical Engineering, vol. 33, no. 12, pp. 1157-1165, December 1986.
[5] S. Yazdani and J. M. Vesin, "Extraction of QRS fiducial points from the ECG using adaptive mathematical morphology," Digital Signal Processing: A Review Journal, vol. 56, pp. 100-109, September 2016.
[6] X. Ning and I. W. Selesnick, "ECG enhancement and QRS detection based on sparse derivatives," Biomedical Signal Processing and Control, vol. 8, no. 6, pp. 713-723, July 2013.
[7] S. Farashi, "A multiresolution time-dependent entropy method for QRS complex detection," Biomedical Signal Processing and Control, vol. 24, pp. 63-71, February 2016.
[8] D. Castells-Rufas and J. Carrabina, "Simple real-time QRS detector with the MaMeMi filter," Biomedical Signal Processing and Control, vol. 21, pp. 137-145, August 2015.
[9] M. R. Homaeinezhad, M. ErfanianMoshiri-Nejad, and H. Naseri, "A correlation analysis-based detection and delineation of ECG characteristic events using template waveforms extracted by ensemble averaging of clustered heart cycles," Computers in Biology and Medicine, vol. 44, pp. 66-75, January 2014.
[10] L. D. Sharma and R. K. Sunkaria, "A robust QRS detection using novel pre-processing techniques and kurtosis based enhanced efficiency," Measurement: Journal of the International Measurement Confederation, vol. 87, pp. 194-204, June 2016.
[11] R. J. Martis, U. R. Acharya, and L. C. Min, "ECG beat classification using PCA, LDA, ICA and discrete wavelet transform," Biomedical Signal Processing and Control, vol. 8, no. 5, pp. 437-448, September 2013.

[12] A. Karimipour and M. R. Homaeinezhad, "Real-time electrocardiogram P-QRS-T detection-delineation algorithm based on quality-supported analysis of characteristic templates," Computers in Biology and Medicine, vol. 52, pp. 153-165, September 2014.

[13] R. Rani, V. S. Chouhan, and H. P. Sinha, "Automated detection of QRS complex in ECG signal using wavelet transform," International Journal of Computer Science and Network Security, vol. 15, no. 1, pp. 1-5, January 2015.

[14] Z. Zidelmal, A. Amirou, M. Adnane, and A. Belouchrani, "QRS detection based on wavelet coefficients," Computer Methods and Programs in Biomedicine, vol. 107, no. 3, pp. 490-496, September 2012.

[15] S. Banerjee, R. Gupta, and M. Mitra, "Delineation of ECG characteristic features using multiresolution wavelet analysis method," Measurement: Journal of the International Measurement Confederation, vol. 45, no. 3, pp. 474-487, April 2012.

[16] A. Kumar and M. Singh, "Optimal selection of wavelet function and decomposition level for removal of ECG signal artifacts," Journal of Medical Imaging and Health Informatics, vol. 5, no. 1, pp. 138-146, February 2015.

[17] A. Kumar and M. Singh, "Robust multiresolution wavelet analysis and window search based approach for electrocardiogram features delineation," Journal of Medical Imaging and Health Informatics, vol. 6, no. 1, pp. 146-156, February 2016.

[18] O. El B 'Charri, R. Latif, K. Elmansouri, A. Abenaou, and W. Jenkal, "ECG signal performance de-noising assessment based on threshold tuning of dual-tree wavelet transform," Biomedical Engineering OnLine, vol. 16, no. 26, pp. 1-18, February 2017.

[19] O. El B'Charri, R. Latif, A. Abenaou, and W. Jenkal, "An efficient wavelet-based feature extraction scheme for electrocardiogram signals," Proc. The International Conf. Wireless Technologies, Embedded and Intelligent Systems, April 2017, pp. 1-4.

[20] A. Grossmann and J. Morlet, "Decomposition of Hardy functions into square integrable wavelets of constant shape," SIAM Journal on Mathematical Analysis, vol. 15, no. 4, pp. 723-736, 1984.

[21] S. G. Mallat, "A theory for multiresolution signal decomposition: the wavelet representation," IEEE Transactions on Pattern Analysis and Machine Intelligence, vol. 11, no. 7, pp. 674-693, July 1989.

[22] M. Vetterli and C. Herley, "Wavelets and filter banks: theory and design," IEEE Transactions on Signal Processing, vol. 40, no. 9, pp. 2207-2232, September 1992.

[23] I. W. Selesnick, R. G. Baraniuk, and N. G. Kingsbury, "The dual-tree complex wavelet transform," IEEE Signal Processing Magazine, vol. 22, no. 6, pp. 123-151, November 2005.

[24] N. G. Kingsbury, "The dual-tree complex wavelet transform: a new technique for shift invariance and directional filters," Proc. the 8th IEEE DSP Workshop,vol. 8, August 1998, p. 86.

[25] E. Castillo, D. P. Morales, A. García, F. Martínez-Martí, L. Parrilla, and A. J. Palma, "Noise suppression in ECG signals through efficient one-step wavelet processing techniques," Journal of Applied Mathematics, vol. 2013, pp. 763903-1-763903-13, May 2013.

[26] S. Liu, Y. Li, X. Hu, L. Liu, and D. Hao, "A novel thresholding method in removing noises of electrocardiogram based on wavelet transform," Journal of Information and Computational Science, vol. 10, no. 15, pp. 5031-5041, October 2013.

[27] D. L. Donoho, "De-Noising by Soft-Thresholding," IEEE Transactions on Information Theory, vol. 41, no. 3, pp. 613-627, May 1995.

[28] G. B. Moody and R. G. Mark, "The MIT-BIH arrhythmia database on CD-ROM and software for use with it," Proc. Computers in Cardiology, IEEE Press, August 2002, pp. 185-188.

[29] A. Demski and M. L. Soria, "ecg-kit: a matlab toolbox for cardiovascular signal processing," Journal of Open Research Software, vol. 4, no. 1, pp. 1-4, April 2016.

[30] J. P. V. Madeiro, P. C. Cortez, J. A. L. Marques, C. R. V. Seisdedos, and C. R. M. R. Sobrinho, "An innovative approach of QRS segmentation based on first-derivative, Hilbert and Wavelet Transforms," Medical Engineering & Physics, vol. 34, no. 9, pp. 1236-1246, December 2012.

[31] M. Yochum, C. Renaud, and S. Jacquir, "Automatic detection of P, QRS and T patterns in 12 leads ECG signal based on CWT," Biomedical Signal Processing and Control, vol. 25, pp. 46-52, November 2016.

[32] C. Li, C. Zheng, and C. Tai, "Detection of ECG characteristic points using wavelet transforms," IEEE Transactions on biomedical Engineering, vol. 42, no. 1, pp. 21-28, January 1995.